Journal of Catalysis 268 (2009) 268–281

Contents lists available at ScienceDirect

Journal of Catalysis

journal homepage: www.elsevier.com/locate/jcat

Study of catalyst deactivation and reaction mechanism of steam reforming, partial oxidation, and oxidative steam reforming of ethanol over Co/CeO_2 catalyst

Sania M. de Lima [a,1], Adriana M. da Silva [a], Lídia O.O. da Costa [a], Uschi M. Graham [b], Gary Jacobs [b], Burtron H. Davis [b], Lisiane V. Mattos [a], Fábio B. Noronha [a,*]

[a] Instituto Nacional de Tecnologia – INT, Av. Venezuela 82, CEP 20081-312, Rio de Janeiro, Brazil
[b] Center for Applied Energy Research, The University of Kentucky, 2540 Research Park Drive, Lexington, KY 40511, USA

ARTICLE INFO

Article history:
Received 29 June 2009
Revised 25 September 2009
Accepted 26 September 2009
Available online 4 November 2009

Keywords:
Hydrogen production
Ethanol steam reforming
Ethanol partial oxidation
Ethanol oxidative steam reforming
Co/CeO_2 catalyst
Deactivation mechanism

ABSTRACT

The mechanisms of Co/ceria catalyst deactivation during steam reforming, oxidative steam reforming, and partial oxidation of ethanol were explored by comparing the results from different characterization techniques with those obtained from catalytic testing in a fixed-bed reactor. The nature of carbon deposition and the reaction conditions played critical roles in determining the extent of a catalyst deactivation. To shed light on the modes of carbon deposition under different reaction conditions, the mechanisms by which the adsorbed surface species turned over on the catalyst surface were evaluated using diffuse reflectance infrared spectroscopy under reaction conditions and temperature-programed desorption of adsorbed ethanol. In steam reforming, ethoxy species were converted to acetate and steam promoted forward acetate demethanation. The resulting methane decomposed on Co metal particles. In this case, carbon diffused through the Co particle, nucleating growth sites for filamentous carbon behind it, with the resulting filaments lifting Co from the support. High H_2O/ethanol ratios and oxygen promoted cleaning of the cobalt surface.

1. Introduction

The environmental goal of decreasing atmospheric CO_2 by switching in part to renewable resources, combined with the relatively low cost of sugar cane and other plant-based resources in certain countries, has been the driving forces behind hydrogen production research aimed at utilizing bio-ethanol as an environmentally benign resource.

Different strategies have been proposed to produce hydrogen from ethanol: steam reforming (SR) (reaction 1); partial oxidation (POX) (reaction 2); and oxidative steam reforming (OSR) (reaction 3) [1].

$$C_2H_5OH + 3H_2O \rightarrow 2CO_2 + 6H_2 \quad (1)$$

$$C_2H_5OH + 1.5O_2 \rightarrow 2CO_2 + 3H_2 \quad (2)$$

$$C_2H_5OH + 2H_2O + 0.5O_2 \rightarrow 2CO_2 + 5H_2 \quad (3)$$

While SR has been extensively studied [2–9], there are few studies in the open literature that focus on the POX [10–13] and OSR [14–17] reactions. The advantage of SR for hydrogen production applications is high hydrogen yield. However, it is a highly endothermic reaction and as such, high operation temperatures are necessary [1]. In addition, large amounts of water are required, implying higher energy consumption requirements for vaporization. An alternative reaction for hydrogen production is POX, an exothermic reaction exhibiting quick start-up and response times. This choice also offers the potential of a more compact reactor design, a desirable feature for mobile fuel cell applications [10]. The main disadvantages are the likelihood of hot-spot formation, making control of the reaction difficult, and low hydrogen yield. OSR, also known as autothermal reforming, combines the SR and POX reactions in one reactor, and thus, if carefully balanced, precludes the need for an external heat supply [14].

Depending on the fuel cell application, one technology may offer potential advantages over another. However, all these technologies face one common drawback: several reaction pathways may occur depending on the reaction conditions and catalyst used. Consequently, some of these reactions lead to the formation of coke, which can in turn induce catalyst deactivation.

The nature of the support and metal directly influences the product distribution and catalyst stability during ethanol conversion reactions [2,3]. In spite of their lower activity relative to the supported metals, metal oxide catalysts can be used to produce hydrogen that is virtually free of CO and with little carbon deposition on the catalyst surface, provided that the appropriate reaction conditions are selected [18–21]. However, a wide range of undesirable by-products (e.g., ethylene, acetaldehyde, and acetone) is

* Corresponding author. Fax: +55 21 2123 1166.
E-mail address: fabio.bellot@int.gov.br (F.B. Noronha).
[1] Present address: Universidade Estadual do Oeste do Paraná – Unioeste, Campus de Toledo, Rua da Faculdade, 645, Jd. La Salle, CEP 85903-000, Toledo, Brazil.

0021-9517/$ - see front matter © 2009 Elsevier Inc. All rights reserved.
doi:10.1016/j.jcat.2009.09.025

formed during SR of ethanol over metal oxides in comparison with the supported metal catalysts, depending on the metal oxide properties.

Al_2O_3 is generally used as a support but its acid sites promote the dehydration of ethanol to ethylene [7]. MgO contains strongly basic sites, which are proposed to be highly active for ethanol dehydrogenation to acetaldehyde [21]. Ceria and ceria-containing mixed oxides have also been proposed to be catalytically active components of supported metal catalysts for ethanol conversion reactions due to their high oxygen storage capacities, suggested to improve catalyst stability [16,22–24], and because of their ability to promote the dissociation of molecules of the type ROH (e.g., H_2O and ethanol) [25]. In addition, the strong metal-support interaction has been postulated to prevent metal particle sintering, which can contribute to catalyst deactivation [26].

Different base metals (Ni, Co, and Cu) and noble metals (Pd, Pt, Rh, and Ru) have been tested for ethanol conversion reactions. Since cobalt is a much less costly alternative to noble metals, Co-based catalysts have been extensively studied for SR [4,17,20,21,26–30], though less so for POX [11] and OSR [17]. In spite of reportedly high activities and selectivities, Co-based catalysts are not immune to the problem of deactivation. In the literature, there are only a few publications dedicated to investigating the root causes of the deactivation of Co-based catalysts [26,31–34] and virtually all of them focus on SR. There are no studies in the literature comparing the causes of catalyst deactivation for the different ethanol conversion reactions (SR, POX, and OSR).

The carbon deposits following SR of ethanol have been studied by Raman spectroscopy, temperature-programed oxidation (TPO), and transmission electron microscopy (TEM), and include both filamentous and amorphous carbon covering the metallic particle and the support [31–34]. TEM images of a deactivated Co/ZnO catalyst after SR revealed Co particles either covered by carbonaceous deposits or located inside carbon filaments [32]. Wang et al. [34] studied the deposition of carbon during SR over Co/CeO_2 as a function of reaction temperature; between 623 and 723 K, where severe deactivation was observed, the cobalt particles were found to be completely encapsulated by coke. They proposed that the active sites responsible for ethanol dehydrogenation were covered by coke and as a result, ethanol is preferentially dehydrated to ethylene. However, the product distribution observed may not correspond to this explanation, as acetaldehyde concentration was found to increase with time on stream (TOS) at 723 K, contrary to the view that the dehydrogenation sites were blocked. When the reaction was carried out at 773 or 823 K, carbon filaments were detected but the catalyst remained quite stable for 8 h TOS. Above 873 K, carbon deposits were no longer detected by TEM analysis. Galeti et al. [33] also studied the effect of reaction temperature on the performance of CuCoZnAl catalyst during SR. The nature of the carbon deposits formed was evaluated by Raman spectroscopy and temperature-programed oxidation experiments. CuCoZnAl rapidly deactivated during SR at 673 and 773 K, whereas the activity remained unchanged at 873 K. Regardless of the reaction temperature used, Raman spectra revealed the presence of two types of carbon: ordered (e.g., graphitic, ordered filamentous) and disordered (e.g., amorphous, defect-laden filamentous) carbon. Scanning electron microscopy (SEM) confirmed the formation of carbon filaments after reaction at 773 K while amorphous carbon was present at 873 K. They proposed that coke was removed from the surface of the catalyst by the reverse Boudouard reaction, improving catalyst stability at this temperature.

Recently, Pereira et al. [17] proposed that the loss of activity of Co-based catalysts is directly related to the oxidation of metallic Co particles during reaction. Co/SiO_2, $Co–Rh/SiO_2$, and $Co–Ru/SiO_2$ catalysts deactivated during OSR carried out between 623 and 673 K. The decrease in ethanol conversion was accompanied by a decrease in hydrogen selectivity and an increase in acetaldehyde selectivity. According to the authors, the surfaces of Co particles were oxidized by oxygen from the feed and the cobalt oxide formed favored the dehydrogenation of ethanol to acetaldehyde. The addition of a noble metal (e.g., Rh, Ru) was suggested to prevent or at least reduce the oxidation of cobalt particles. It is important to stress that the oxidation state of cobalt was not investigated by surface techniques such as X-ray photoelectron spectroscopy (XPS) or XANES. Raman spectroscopy results demonstrated the presence of two types of carbon after reaction, which were removed by oxygen treatment after OSR.

Therefore, the mechanism of Co-based catalyst deactivation is still unclear. The aim of this work is to perform a systematic study of the deactivation mechanism of Co/ceria catalysts during the different ethanol conversion reactions. To achieve this goal, the reactions mechanisms of SR, POX, and OSR over Co/CeO_2 catalyst were first investigated using a combination of reaction testing, temperature-programed desorption (TPD), and diffuse reflectance infrared Fourier transform spectroscopy (DRIFTS) measurements recorded under in situ reaction conditions. In addition, high-resolution transmission electron microscopy (HR-TEM), scanning transmission electron microscopy (STEM) and thermogravimetric analysis (TG) were employed to characterize the carbonaceous deposits formed. Finally, a deactivation mechanism is proposed.

2. Experimental

2.1. Catalyst preparation

Cerium oxide was prepared by calcination of cerium (IV) ammonium nitrate at 1073 K (CeO_2). Cobalt was added to the CeO_2 support by incipient wetness impregnation using an aqueous solution of $Co(NO_3).6H_2O$. After impregnation of 10 wt.% cobalt, the samples were dried at 373 K and calcined under flowing air (50 mL/min) at 673 K, for 2 h.

2.2. BET surface area

The BET surface areas of the samples were measured using a Micromeritics ASAP 2020 analyzer by nitrogen adsorption at the boiling temperature of liquid nitrogen.

2.3. X-ray diffraction (XRD)

XRD measurements were recorded using a RIGAKU diffractometer employing CuKα radiation (λ = 1.5406 Å). Data were collected over the 2θ range of 25–75° using a scan rate of 0.04°/step and a scan time of 1 s/step. Scherrer equation was used to estimate the crystallite mean diameter based on the reflection (311) of Co_3O_4 particles.

2.4. Temperature-programed reduction (TPR)

The catalyst was pretreated at 473 K for 1 h under a flow of argon prior to the TPR experiment in order to remove traces of water. The reducing mixture (1.5% hydrogen in argon) was passed through the sample (300 mg) at a flow rate of 30 mL/min and the temperature was increased to 1273 K at a heating rate of 10 K/min.

2.5. Diffuse reflectance spectroscopy (DRS)

Diffuse reflectance spectra of a Co/CeO_2 catalyst and a reference compound were recorded between 200 and 800 nm on a UV–Vis NIR spectrometer (Cary 5 - Varian) equipped with a Harrick integrating sphere using the support as a reference.

2.6. TPD of ethanol

TPD experiments of adsorbed ethanol were carried out in a micro-reactor coupled to a quadrupole mass spectrometer (Omnistar, Balzers). Prior to TPD analyses, the samples were reduced under flowing H_2 (30 mL/min) by ramping to 1023 K (10 K/min) and holding at this temperature for 1 h. After reduction, the system was purged with helium at 1023 K for 30 min and cooled to room temperature. The adsorption of ethanol was carried out at room temperature using an ethanol/He mixture, which was obtained by flowing He through a saturator containing ethanol at 298 K. After adsorption, the catalyst was heated at 20 K/min to 773 K under flowing helium (60 mL/min). The products were monitored using a quadrupole mass spectrometer.

2.7. DRIFTS

DRIFTS spectra were recorded using a Nicolet Nexus 870 spectrometer equipped with a DTGS-TEC detector. A Thermo Spectra-Tech cell capable of high pressure/high temperature operation and fitted with ZnSe windows served as the reaction chamber for in situ adsorption and reaction measurements. Scans were taken at a resolution of 4 to give a data spacing of 1.928 cm^{-1}. The number of scans taken was 512. The amount of catalyst was ~40 mg.

Samples were first pre-reduced in an external fixed-bed reactor using 200 mL/min H_2:He (1:1) by increasing the temperature at 10 K/min to 1023 K, holding at this temperature for 1 h, and cooling to room temperature. The reactor was purged with helium prior to switching to 1%O_2/He (25 ml/min) for 4 h to passivate the sample. Samples were re-reduced in situ by flowing 200 ml/min H_2:He (1:1) and increasing the temperature at 10 K/min to 773 K and holding at this condition for 1 h. The catalyst was purged in flowing He at 773 K, prior to cooling in flowing He to 313 K.

For ethanol adsorption and SR reaction tests, He was bubbled at ~15 mL/min through a saturator filled with ethanol and held at 273 K. For SR tests, a second helium stream (~15 mL/min) was bubbled through a saturator filled with water and held at 298 K. The two streams were joined at a tee-junction, prior to which 1 psig check valves were placed on the lines to prevent a back-flow condition. The saturator gas flows and temperatures were set to provide a H_2O:CH_3CH_2OH stoichiometric ratio of 2:1. Adsorption/reaction measurements were started at 323 K, and then the temperature was increased at 10 K/min; measurements were recorded at 373, 473, 573, 673, and 773 K.

For POX, 30 mL/min of 0.75% O_2/He was bubbled through a saturator filled with ethanol held at 273 K. For OSR, 15 mL/min of ~0.75%O_2/He was bubbled through the H_2O saturator held at 298 K and another 15 mL/min of 0.75% O_2/He was bubbled through an ethanol saturator held at 273 K. The two streams were combined at a tee-junction, prior to which 1 psig check valves were added to prevent the possibility of back-flow. The same temperatures and ramp rates were used as in SR.

2.8. TG analysis

TPO experiments were performed using a TA Instruments TGA analyzer (SDT Q 600) in order to determine the amount of carbon formed over the catalyst. Approximately 10 mg of spent catalyst was heated under air flow from room temperature to 1273 K at a heating rate of 20 K/min and the weight change was measured.

2.9. Transmission electron microscopy

HR-TEM and STEM investigations were conducted with a 200-keV JEOL-2010f field-emission electron microscope equipped with an Oxford energy-dispersive X-ray detector, a STEM unit and a Gatan imaging filter. TEM images were recorded with a Gatan 794 slow-scan charge coupled device (CCD) camera. Prior to the investigations, minute quantities of powdered sample material were dispersed onto copper grids equipped with lacey carbon support structures.

2.10. Reaction conditions

Direct ethanol decomposition (ED), SR, POX, and OSR were performed in a fixed-bed reactor at atmospheric pressure. Prior to reaction, catalysts were reduced under pure hydrogen (30 mL/min) at 1023 K for 1 h and then purged under N_2 at the same temperature for 30 min. All reactions were carried out at 773 K except for SR, which was also performed at 1073 K. POX was conducted using an O_2/ethanol molar ratio of 0.5. The choice of O_2/ethanol ratio was based on the work of Cavallaro et al. [35], who showed that the ethanol conversion is around 100% and the H_2 production reaches a maximum using an O_2/ethanol ratio between 0.4 and 0.5. For SR, H_2O/ethanol molar ratios of 3.0 and 10.0 were utilized. OSR was performed employing a H_2O/ethanol molar ratio of 3.0 and an O_2/ethanol molar ratio of 0.5. The reactant mixtures were obtained using two saturators containing water and ethanol, which were maintained at the temperature required to obtain the desired H_2O/ethanol and O_2/ethanol molar ratios. For ED and POX, N_2 (30 mL/min) and 5.6% O_2/N_2 mixture (30 mL/min), respectively, were passed through the saturator with ethanol, and then the reactant mixtures obtained were diluted with N_2 (each N_2 stream flowed at 30 mL/min). In the case of SR, the reactant mixture was obtained by flowing two N_2 streams (30 mL/min) through each saturator containing ethanol and water separately. For OSR, a flow of 5.6% O_2/N_2 (30 mL/min) and a flow of N_2 (30 mL/min) were passed through the saturators containing ethanol and water, respectively. The partial pressure of ethanol was maintained constant for all experiments. The variation of partial pressure of water was compensated by a decrease in the partial pressure of N_2.

In order to observe the catalyst deactivation within a short timeframe, a small amount of catalyst was used (20 mg). The samples were diluted with inert SiC (SiC mass/catalyst mass = 3.0). The reaction products were analyzed by gas chromatography (Micro GC Agilent 3000 A) containing two channels for dual thermal conductivity detectors (TCDs) and two columns: a molecular sieve and a Poraplot U column. The ethanol conversion and selectivity to products were determined from:

$$X_{\text{ethanol}} = \frac{(n_{\text{ethanol}})_{\text{fed}} - (n_{\text{ethanol}})_{\text{exit}}}{(n_{\text{ethanol}})_{\text{fed}}} \times 100 \quad (4)$$

$$S_x = \frac{(n_x)_{\text{produced}}}{(n_{\text{total}})_{\text{produced}}} \times 100 \quad (5)$$

where $(n_x)_{\text{produced}}$ = moles of x produced (x = hydrogen, CO, CO_2, methane, acetaldehyde, or ethylene) and $(n_{\text{total}})_{\text{produced}}$ = moles of H_2 + moles of CO + moles of CO_2 + moles of methane + moles of acetaldehyde + moles of ethylene (i.e., the moles of water produced are not included).

3. Results and discussion

3.1. Catalyst characterization

The BET surface area of the CeO_2 support was very low (9.9 m^2/g) and not measurably affected by the addition of cobalt (9.8 m^2/g). The X-ray diffraction pattern of Co/CeO_2 displayed the main lines characteristic of CeO_2 ($2\theta = 28.5°$, 47.5°, and 56.4°) and Co_3O_4 ($2\theta = 36.8°$ and 65.4°) (Fig. 1a). The peak broadening procedure was used to estimate the mean Co_3O_4 crystallite size by Scherrer

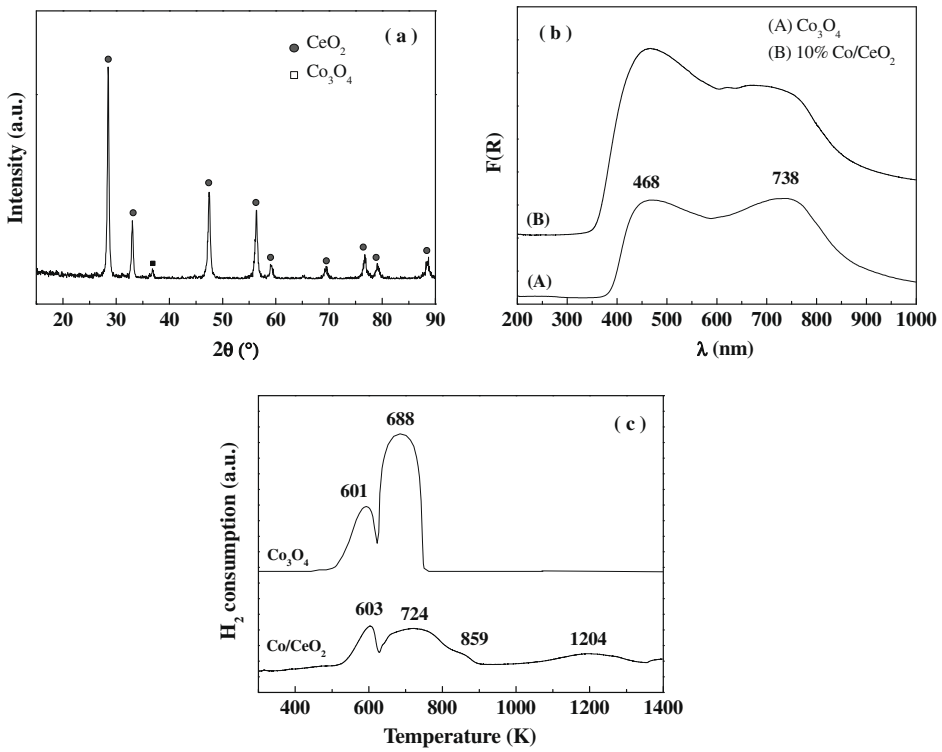

Fig. 1. (a) XRD pattern of Co/CeO_2 catalyst; (b) DRS spectra of the Co/CeO_2 catalyst and Co_3O_4; (c) TPR profile of Co/CeO_2 catalyst.

equation. The calcined sample exhibited a Co_3O_4 crystallite size of 19 nm. The DRS spectra obtained from the Schuster–Kubelka–Munk (SMK) equation for Co_3O_4 and Co/CeO_2 catalysts are presented in Fig. 1b. The spectrum of Co_3O_4 presented bands at 470 and 734 nm. The DRS spectrum of Co/CeO_2 catalyst exhibited two bands at 468 and 738 nm. A comparison between the DRS spectra of the Co/CeO_2 catalyst and reference compound suggests that cobalt in the calcined Co/CeO_2 catalyst must be present, for the most part, as Co_3O_4. The bands around 468 and 738 nm could be attributed to octahedral Co^{3+} [36,37]. The TPR profiles of Co_3O_4 and Co/CeO_2 are presented in Fig. 1c and are in agreement with the DRX and DRS results. The TPR profile of Co_3O_4 presents two hydrogen uptakes at 601 and 688 K, indicating that reduction occurs in two steps: $Co_3O_4 \rightarrow CoO \rightarrow Co^{\circ}$ (Fig. 1c) [37]. The reduction profile of Co/CeO_2 catalyst exhibits two peaks at 603 and 724 K that correspond to the two-step reduction of Co_3O_4 particles. This result indicates that the Co/CeO_2 catalyst mainly comprises supported Co_3O_4 particles. However, we cannot rule out the presence of a small fraction of Co^{2+} probably linked to the support. The broad reduction peak at around 700–800 K could also comprise the reduction of Co^{2+} species. In addition to the peaks corresponding to the reduction of Co_3O_4, a shoulder was detected at around 859 K as well as a small peak at 1204 K. The H_2 uptake at 859 K is attributed to the surface reduction of CeO_2, while the H_2 consumption at around 1204 K is related to the formation of bulk Ce_2O_3. Reduction of Co oxides to metal occurs along with the reduction of the surface shell of ceria, which is promoted by the presence of the cobalt metal, and is located in the broad peak between 700 and 800 K [38]. One view is that, during activation, the metal can facilitate reduction of the surface shell of ceria from Ce^{4+} to Ce^{3+} by H_2 dissociation and spillover, leading to the production of bridging OH groups on the surface associated with reduced Ce^{3+} centers. The bridging OH groups can be interpreted to be dissociated H_2O located at an O vacancy. Reduction at 1023 K will likely completely reduce the ceria surface shell, as well as a fraction of the subsurface layers.

3.2. Reaction mechanism

3.2.1. TPD of ethanol

Fig. 2 presents the TPD profiles of adsorbed ethanol for the Co/CeO_2 catalyst. At low temperatures, Co/CeO_2 catalyst exhibited the simultaneous formation of H_2 and CH_4 (397 K). Moreover, ethanol desorption and CO production were not detected within this temperature range. Some authors [12,39,40] observed the formation of H_2, CH_4, and CO in the low-temperature region during TPD of ethanol over Al_2O_3- and CeO_2-supported metals. They suggested that

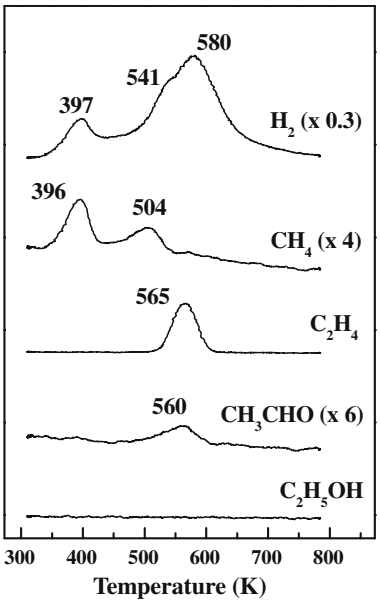

Fig. 2. TPD profiles of ethanol desorption obtained for Co/CeO_2 catalyst.

ethanol adsorbs on the catalyst surface as ethoxy species that can be decomposed to H_2, CH_4, and CO over metal particles. The absence of CO desorption in our work suggests that CO still remained adsorbed in this range of temperature.

At high temperatures, significant peaks for H_2 production (541 and 580 K) and a much smaller peak for CH_4 formation (504 K) were detected. In addition, peaks corresponding to acetaldehyde and ethylene formation were observed at 560 and 565 K, respectively. Erdohelyi et al. [8] also observed the production of ethylene and acetaldehyde at around 500 K over CeO_2- and Al_2O_3-supported noble metal catalysts. In that case, ethylene and acetaldehyde were suggested to be produced by dehydration and dehydrogenation of ethanol, respectively. No significant peaks for CO, CO_2, crotonaldehyde, acetone, or benzene were observed by TPD analysis. According to the literature [12,39], the formation of CO and CH_4 at high temperatures (above 500 K) during TPD of ethanol over CeO_2 and Al_2O_3 supports is due to the decomposition of carbon species (e.g., acetaldehyde and acetate species) previously formed. Recalling that acetate species are formed by oxidation of the dehydrogenated species, a fraction of the acetate species can be oxidized to carbonate species that are, in turn, decomposed to CO_2. Then, in this work, the small peak for CH_4 and the absence of CO and CO_2 at high temperatures suggest that the formation of acetate species was not favored over Co/CeO_2 catalyst during ethanol TPD.

Finally, the large production of H_2 detected at high temperatures in the TPD profiles of the Co/CeO_2 catalyst can be assigned to the desorption of H_2 previously formed during the different steps of ethanol dehydrogenation.

3.2.2. DRIFTS analysis of ethanol desorption

Fig. 3 shows the IR spectra of adsorbed ethanol on Co/CeO_2 catalyst at different temperatures. At room temperature, the bands at 1049, 1087, 1356, 1406, 1444, 2862, 2925, and 2969 cm^{-1} correspond to different vibrational modes of ethoxy species, which were formed by dissociative adsorption of ethanol over Ce cations [12,41,42]. In addition to the bands of ethoxy species, there are also bands at 1265, 1624, and 1892 cm^{-1}. The bands at 1265 and 1624 cm^{-1} are assigned to molecularly adsorbed ethanol [42] and to the ν(CO) vibrational mode of acetyl species [43], respectively. The acetyl species are produced by the dehydrogenation of ethoxy species via acetaldehyde. The band at 1892 cm^{-1} corresponds to the ν(CO) stretching mode of bridge-bonded CO adsorbed on Co particles [44].

When the catalyst was heated to 373 and 473 K, the intensity of the bands corresponding to ethoxy species decreased and the band related to molecularly adsorbed ethanol was no longer detected. Furthermore, the bands assigned to acetaldehyde (1650 and 1713 cm^{-1}) were observed [12]. This result confirms that a fraction of ethanol decomposes to H_2, CH_4, and CO and another fraction dehydrogenates to acetaldehyde, as suggested by TPD analysis.

At 573 K, weak bands were observed at 1342, 1431, and 1533 cm^{-1} corresponding to the $\delta_s(CH_3)$, $\nu_s(OCO)$, and $\nu_a(OCO)$ vibrational modes of acetate species, respectively [12,41,42]. Moreover, the bands corresponding to acetaldehyde were no longer detected. The transformation from ethoxy species to acetate species involves the dehydrogenation of ethoxy species to acetaldehyde, which may be further dehydrogenated to acetyl species. Erdohelyi et al. [8] suggested that acetate species are formed via two reaction pathways: (i) the reaction between the acetyl species and oxygen from the support; and/or (ii) the reaction of acetaldehyde with surface OH groups. Since the Co/CeO_2 catalyst was previously reduced at 1023 K, the acetate species were likely produced from the reaction between adsorbed acetaldehyde and surface OH groups. Increasing the temperature to 673 K led to a significant decrease in the bands related to acetate species. At 773 K, the bands of acetate species were no longer detected. These results indicate that the formation of acetate species was not favored over Co/CeO_2 catalyst for the ED reaction, consistent with the decomposition products arising during TPD.

Recently, Song and Ozkan [45] carried out DRIFTS experiments after ethanol adsorption over a Co/CeO_2 catalyst. The spectra revealed the presence of acetate species even at room temperature, attributed to the large availability of oxygen from the ceria support. The difference between their work and ours likely stems from the difference in reduction temperature used in each work. We previously reduced our catalyst under pure hydrogen at 1023 K in order to assure the complete reduction of cobalt oxides, the surface shell reduction of ceria, and the reduction of a fraction of subsurface ceria, as previously discussed in the section on TPR. On the other hand, Song and Ozkan [45] reduced the catalyst with a H_2/He mixture at 673 K, which likely only facilitates surface shell reduction. Thus, the amount of oxygen on the support may be higher in reference [45], owing to the diffusion of subsurface O to the sur-

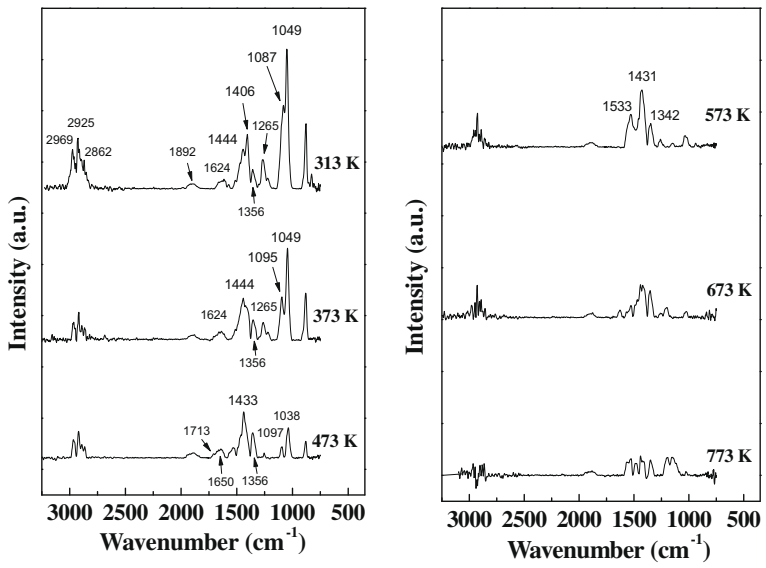

Fig. 3. DRIFTS spectra of adsorbed ethanol obtained on Co/CeO_2 catalyst at different temperatures.

face, and thereby favoring the oxidation of ethoxy species to acetate.

3.2.3. DRIFTS analysis under reaction conditions

Figs. 4–6 display DRIFTS results of the impact of temperature on SR, POX, and OSR, respectively. It is noteworthy that there are no DRIFTS experiments reported in the literature carried out under reaction conditions over supported cobalt catalysts. We have recently demonstrated that IR experiments under reaction conditions are fundamental to obtain reliable mechanistic information that more closely reflects the reaction conditions of the true catalytic test [16].

3.2.3.1. DRIFTS analysis under ethanol + water mixture. In Fig. 4, which covers SR, at low temperature (e.g., 313 K), the coverage of partially reduced ceria is dominated by ethoxy species (main bands: ν(CO) = 1057, 1101 cm^{-1} and ν(CH) = 2881, 2974 cm^{-1}) resulting from the dissociative adsorption of ethanol. Even at low temperature, some acetate species are clearly present (ν_s(OCO) = 1425 cm^{-1}; ν_{as}(OCO) = 1556 cm^{-1}), indicating that in the presence of water acetate formation is favored. When the temperature was steadily increased to 373, 473, and 573 K, the intensities of ethoxy bands clearly decreased, whereas those of acetate species (1552–1558 cm^{-1} and 1425–1433 cm^{-1}) increased.

At 573 K, the different branches of the gas-phase CO_2 band (~2350 cm^{-1}) are detected, and the intensity is higher at 673 and 773 K. The intensity of acetate bands significantly decreased in moving from 573 to 673 K. At 673 K, new bands in addition to those related to acetate species, likely corresponding to carbonate complexes, are detected in the ν(OCO) stretching range; the coverage of all species is quite low at 773 K.

Comparing these results with the spectra obtained during ethanol desorption (Fig. 3) significant differences in the relative band

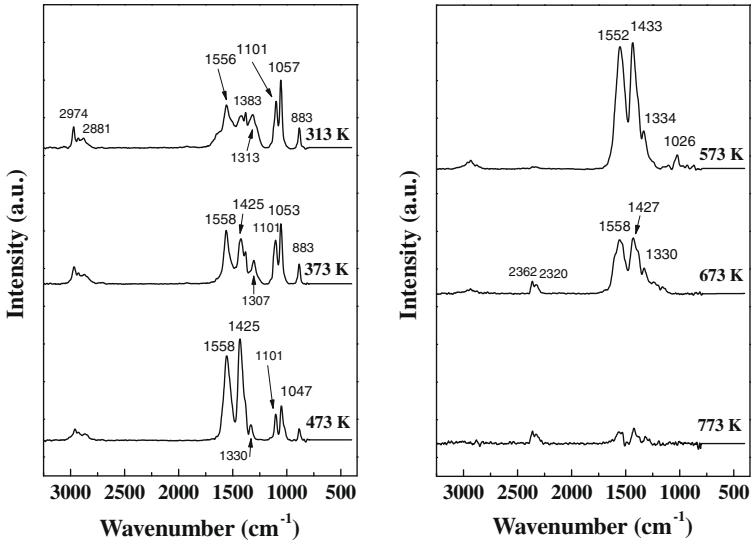

Fig. 4. DRIFTS spectra obtained on Co/CeO_2 catalyst at different temperatures and under the reaction mixture containing ethanol and water (H_2O/ethanol ratio = 2.0).

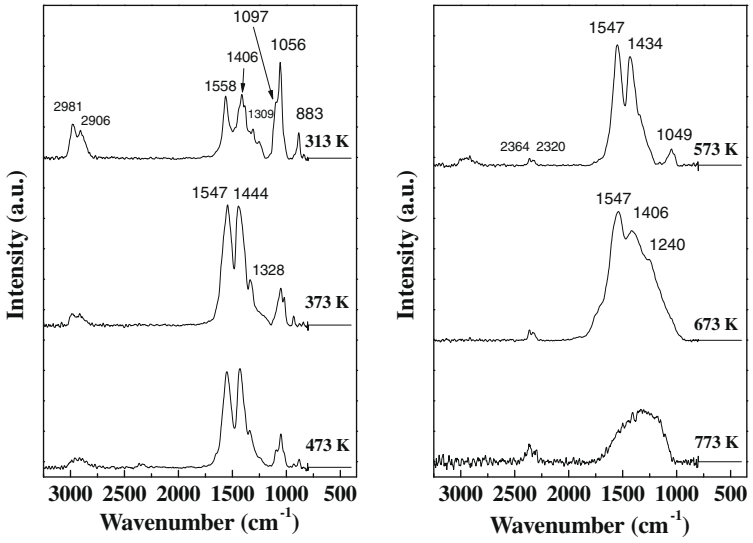

Fig. 5. DRIFTS spectra obtained on Co/CeO_2 catalyst at different temperatures and under the reaction mixture containing ethanol and oxygen (oxygen/ethanol ratio = 0.5).

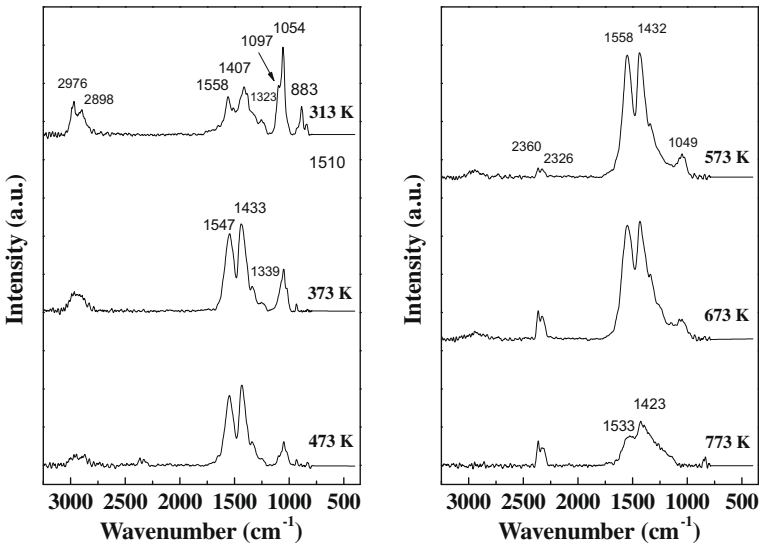

Fig. 6. DRIFTS spectra obtained on Co/CeO_2 catalyst at different temperatures and under the reaction mixture containing ethanol, water, and oxygen (H_2O/ethanol ratio = 2.0; oxygen/ethanol ratio = 0.5).

intensities are observed. Adding water to the feed promoted the formation of acetate species as well as the acetate decomposition reaction, in agreement with our previous study [16].

3.2.3.2. DRIFTS analysis under an ethanol + oxygen mixture. A similar pattern emerges with POX (Fig. 5). At low temperature (313 K), there are ethoxy species (main bands: ν(CO) = 1056, 1097 cm^{-1} and ν(CH) = 2906, 2981 cm^{-1}) while acetate is now present (ν_{as}(OCO) = 1558 cm^{-1}). Increasing temperature to the 373–573 K range led to a decrease in the coverage of ethoxy species and a significant increase in the coverage of acetate species; moreover, the acetate bands appear to be of higher intensity relative to the case of SR (i.e., compare Fig. 5 with Fig. 4). CO_2 can be detected at lower temperature (473 K) than previously observed with SR (573 K). At 673 K, both acetate and carbonate bands are observed, and their coverages are higher than observed during SR at the same temperature. The results suggest that H_2O plays an important role in the decomposition of acetate species, and one can speculate based on the reactivity data that both the decomposition rate and selectivity to acetate are influenced by the presence/absence of H_2O. At 773 K, it appears that some carbonate is present, as ν(OCO) bands are detected in the broad range of 1000–1700 cm^{-1}.

We have recently reported DRIFTS results under POX conditions over $Pt/CeZrO_2$ catalyst. The addition of oxygen was suggested to promote the oxidation of ethoxy species to acetate species via reaction with support oxygen adatoms, as vacancies of the support could be continuously replenished by oxygen from the feed. In addition, the bands corresponding to carbonate species were more intense when the ethanol–oxygen mixture was used. The current results are in accordance with our previous findings [16].

3.2.3.3. DRIFTS analysis under ethanol + water + oxygen mixture. Similar trends emerge with OSR (Fig. 6). At low temperature (313 K), ethoxy species (main bands: ν(CO) = 1054, 1097 cm^{-1} and ν(CH) = 2898, 2976 cm^{-1}) dominate the coverage while some acetate is already present [ν_{as}(OCO) = 1558 cm^{-1}]. Increasing temperature to the 373–573 K range led to decreases in the intensities of bands corresponding to ethoxy species and increases in the band intensities of surface acetate. In addition, the spectra reflect a composite between the DRIFTS spectra recorded under SR conditions and those obtained during POX. CO_2 can be detected at lower temperature (473 K) than previously observed with SR (573 K), but essentially at the same temperature observed with POX. At 673 K, bands corresponding to both acetate and carbonate are observed, and the coverages of these species are apparently higher than those observed with SR but lower than the ones found with POX at the same temperature. There appears to be a higher surface concentration of acetate species relative to carbonate during OSR than observed under POX conditions, since weak bands at around 2850 cm^{-1} corresponding to the main ν(CH) vibrational stretching modes are still observed in the DRIFTS spectrum during OSR. At 773 K, it seems that mainly carbonate is present, as ν(OCO) bands are detected in the broad range of 1000–1700 cm^{-1}. To our knowledge, these are the first DRIFTS spectra under OSR reaction conditions reported in the literature for supported cobalt catalysts.

The DRIFTS results are better explained in the context of our earlier proposed mechanism for SR of ethanol over Pt/CeO_2 and Pt/CeO_2–ZrO_2 catalysts [16,25].

In the proposed mechanism (Scheme 1), which includes a junction effect with the support, ethoxy species are generated on the surface of partially reduced ceria by dissociative adsorption. Oxidative dehydrogenation via support –OH groups generates the acetate intermediate, liberating H_2 in the process at the support-metal interface [16]. In POX and OSR, the dehydrogenated species may react with oxygen from the support to produce the acetate species. In the presence of coadsorbed H_2O, the acetate decomposition reaction is favored, producing CO_x and CH_x species.

3.3. Reactions

3.3.1. ED, SR, POX, and OSR at 773 K over Co/CeO_2

The performance of the Co/CeO_2 catalyst for ED, SR, POX, and OSR reactions at 773 K was evaluated and the results are displayed in Fig. 7a–d. Initial ethanol conversion for ED was approximately 65% but significantly increased to 100% when water (SR), oxygen (POX), or both (OSR) were added to the feed. Kugai et al. [14] also compared the performance of $Ni–Rh/CeO_2$ catalyst on a series of hydrogen production reactions: ED, SR, POX, and OSR. The addition of water, oxygen, or both to the ethanol feed also increased ethanol conversion, and this finding was attributed to a higher propensity for C–C bond cleavage in the presence of water and/or oxygen. Cai et al. [22] carried out a comparative study of SR, POX, and OSR

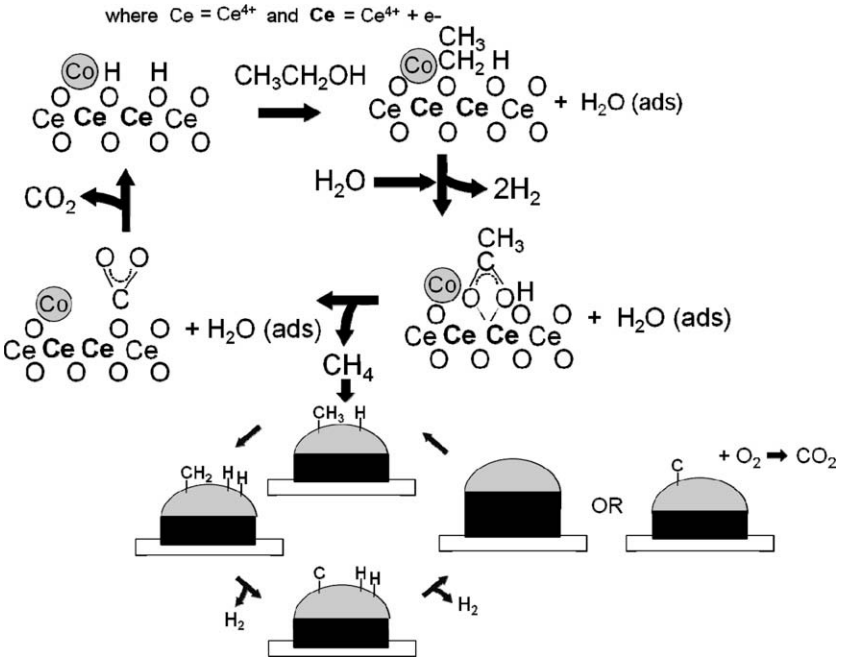

Scheme 1. Reaction mechanism proposed for the ethanol conversion reactions.

reactions over Ir/CeO_2. Ethanol conversion rates for POX and OSR were higher than that for SR, indicating that oxygen promoted the surface reaction of ethanol. They proposed that the lattice oxygen atoms of ceria should assist in activating the ethanol molecule. We previously reported that initial ethanol conversion rates for SR, POX, and OSR reactions over $Pt/CeZrO_2$ were higher than those detected for the ED reaction [16].

Ethanol conversion significantly decreased at the beginning of the SR reaction tests while oxygen addition to the feed significantly improved catalyst stability. Although a different catalyst system was used, Fierro et al. [15] reported that the introduction of a higher amount of oxygen increased the stability of $Ni–Cu/SiO_2$ catalysts during OSR.

The selectivity to hydrogen decreased at the beginning of the ED and POX reaction tests, while it remained constant for the SR and OSR runs. After the first 2 h of TOS, H_2 production remained approximately constant for all the different reactions tested. In addition, hydrogen selectivity increased in the following order: POX < OSR < SR, indicating that oxygen addition likely leads to the production of water. The selectivities to CO and CH_4 were relatively constant during SR, POX, and OSR tests. However, the production of CO and CH_4 was negligible after 1 h TOS for ED, indicating that the ED reaction to CO and CH_4 was no longer observed. The selectivity to CO_2 increased as oxygen was introduced in the feed and was higher in the case of POX. This result indicates that the ethanol combustion reaction occurs when oxygen is added to the feed.

The selectivity to acetaldehyde slightly increased during the first 3 h of TOS and then leveled off at approximately 5% in the cases of SR and OSR. On the other hand, a higher amount of acetaldehyde was formed during ED and POX. The latter result regarding POX agrees well with the findings of Kugai et al. [14], who proposed that oxygen takes part in ethanol dehydrogenation to acetaldehyde rather than C–C bond rupture. We also previously reported that the introduction of oxygen in the feed favors acetaldehyde production during ethanol reforming reactions over $Pt/CeZrO_2$ [16]. Significant amounts of ethene were only detected during ED and its selectivity continuously increased during 6 h of TOS. Dömök et al. [46] reported a decrease in ethene production when the H_2O/ethanol molar ratio in the feed increased during SR of ethanol over alumina-supported Pt catalysts. Ethene is produced by ethanol dehydration over the support as described by reaction (6) and, as such, addition of water inhibits dehydration of ethanol.

$$C_2H_5OH \rightarrow C_2H_4 + H_2O \quad (6)$$

The effect of the H_2O/ethanol molar ratio during SR at 773 K was also evaluated. Ethanol conversion and product distributions as a function of TOS obtained for Co/CeO_2 catalyst during SR with a H_2O/ethanol molar ratio of 10.0 are shown in Fig. 8. Increasing the H_2O/ethanol molar ratio from 3.0 (Fig. 7b) to 10.0 (Fig. 8) significantly promoted long-term catalyst stability. The final ethanol conversion for SR under a H_2O/ethanol molar ratio of 10.0 remained around 100% during 50 h TOS and it was higher than when the H_2O/ethanol molar ratio was 3.0 (52%). Increasing the H_2O/ethanol molar ratio from 3.0 to 10.0 resulted in a decrease in the selectivity to methane and CO while acetaldehyde formation was no longer observed.

Recently, we demonstrated that the support plays an important role in the SR reaction mechanism [10]. In order to decouple the role of the support from the metal, the SR reaction was carried out over the ceria support alone. Fig. 9 shows the ethanol conversion and product distributions obtained for the CeO_2 support during SR at 773 K, using a H_2O/ethanol molar ratio of 3.0. Ethanol conversion slightly decreased during 6 h of TOS (from 55% to 50%). This is precisely the same final ethanol conversion achieved by the Co/CeO_2 catalyst after the deactivation period (Fig. 7b). The similarity between the final ethanol conversion of Co/CeO_2 and unpromoted CeO_2 suggests that the deactivation is likely due to the loss of activity of the metallic phase.

Regarding the product distributions, hydrogen, CO_2, and ethene were the main products obtained over unpromoted CeO_2. Small quantities of acetaldehyde (≈5%) and trace amounts of methane were also observed. In addition, the production of CO during testing of the unpromoted CeO_2 catalyst was very low (<200 ppm).

3.3.2. Effect of the reaction temperature on SR over Co/CeO_2

SR was also carried out at high temperature (1073 K) and the results are presented in Fig. 10. The catalyst exhibited the same ini-

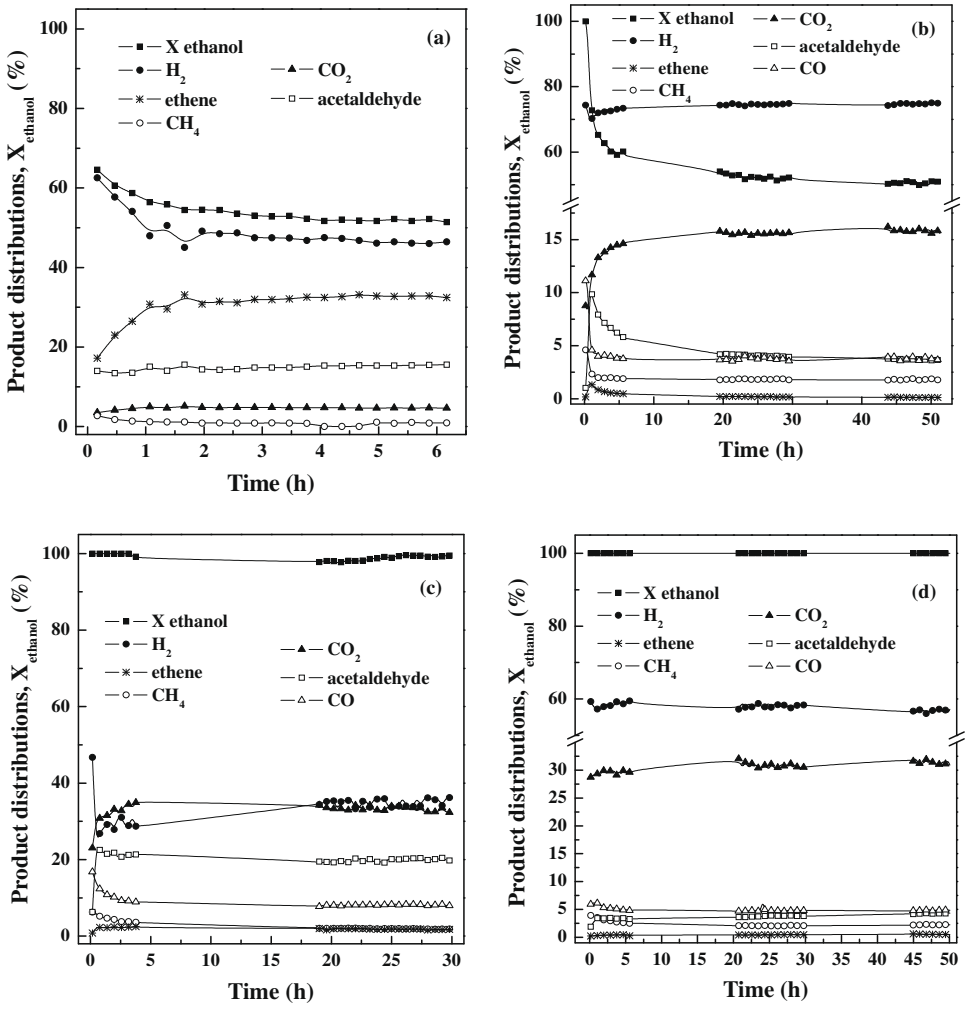

Fig. 7. Ethanol conversion ($X_{ethanol}$) and product distributions versus TOS over Co/CeO_2 catalyst obtained during (a) ED; (b) SR under H_2O/ethanol molar ratio = 3.0; (c) POX under O_2/ethanol = 0.5; and (d) OSR under H_2O/ethanol molar ratio = 3.0 and O_2/ethanol molar ratio = 0.5 (mass of catalyst = 20 mg; $T_{reaction}$ = 773 K and residence time = 0.02 g s/mL).

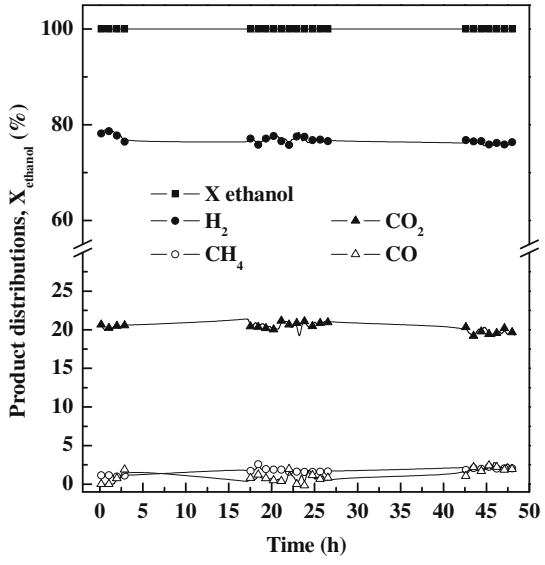

Fig. 8. Ethanol conversion ($X_{ethanol}$) and product distributions versus TOS over Co/CeO_2 catalyst obtained during SR under H_2O/ethanol molar ratio = 10.0 (mass of catalyst = 20 mg; $T_{reaction}$ = 773 K and residence time = 0.02 g s/mL).

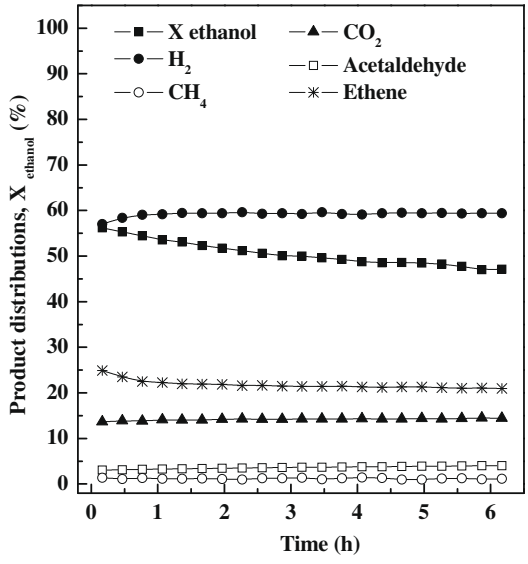

Fig. 9. Ethanol conversion ($X_{ethanol}$) and product distributions versus TOS over unpromoted CeO_2 obtained during SR under H_2O/ethanol molar ratio = 3.0 (mass of catalyst = 20 mg; $T_{reaction}$ = 773 K and residence time = 0.02 g s/mL).

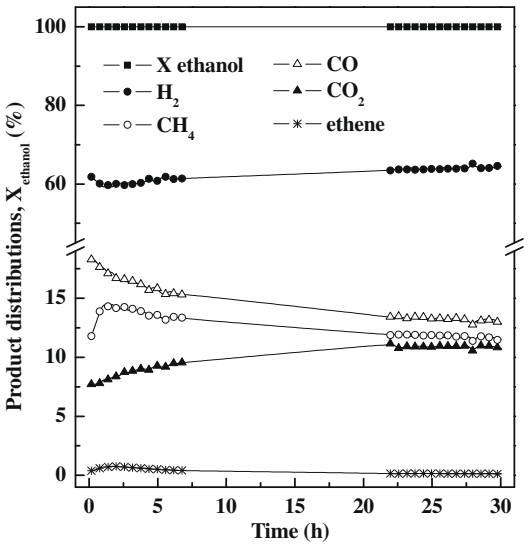

Fig. 10. Ethanol conversion ($X_{ethanol}$) and product distributions versus TOS over 10% Co/CeO_2 catalyst obtained during SR under H_2O/ethanol molar ratio = 3.0 (mass of catalyst = 20 mg; $T_{reaction}$ = 1073 K and residence time = 0.02 g s/mL).

tial ethanol conversion level at both temperatures (Fig. 7b: 773 K and Fig. 10: 1073 K). However, increasing the reaction temperature from 773 to 1073 K greatly improved the stability of the catalyst, such that it remained quite stable at the higher temperature. Concerning product distributions, H_2, CO, CO_2, and CH_4 were the only products detected at high temperature, whereas acetaldehyde was also observed during the run at 773 K. When reaction temperature was increased, the selectivities to H_2 and CO_2 decreased while the selectivities to CO and CH_4 increased. Galetti et al. [33] carried out SR at different temperatures (673, 773, and 873 K) over a CuCoZnAl catalyst. They also observed an improvement in catalyst stability and increases in selectivities to CO and CH_4 as the reaction temperature was risen. Moreover, TG analysis revealed a decrease in the amount of carbon formed upon increasing reaction temperature, in good agreement with the activity test. They proposed that the occurrence of the reverse of Boudouard reaction (Eq. 7) at 873 K improved the resistance of the catalyst to carbon deposition. In another study, the deposition of carbon over Co/CeO_2 was not detected by either TG or TEM analysis when SR was carried out above 873 K [34]. According to Wang et al. [34], the absence of carbon deposition was attributed to the occurrence of steam and CO_2 reforming reactions.

Catalyst stability is probably the most important issue during ethanol conversion reactions to produce hydrogen. Most authors in the open literature report that carbon formation is the main cause of catalyst deactivation, and that the deleterious impact of carbon deposits on catalyst stability depends on both the reaction conditions and the catalyst used. In the next section, the main drivers of catalyst deactivation observed in this work will be discussed in greater detail for all the ethanol conversion reactions. To our knowledge, studies comparing the modes of deactivation during SR, POX, and OSR over Co-based catalysts have not yet been reported.

3.4. Catalyst deactivation

There are three main reactions that may contribute to carbon formation [46–48].

$$2CO \rightarrow C + CO_2 \quad (7)$$

$$CO + H_2 \rightarrow H_2O + C \quad (8)$$

$$CH_4 \rightarrow 2H_2 + C \quad (9)$$

Low reaction temperatures favor the formation of carbon through reactions (7) (Boudouard reaction) and (8) (reverse of carbon gasification). However, carbon formation via reaction (9) (methane decomposition) is the main route at high temperature.

The mechanism of coke formation over supported Ni catalysts during steam reforming of methane is well described in the literature [1,47–49]. Methane dissociates on nickel surface, producing highly reactive carbon species [47]. This carbon may undergo a number of processes, including (1) reaction with water; (2) encapsulation of the Ni particle surface; or (3) dissolution in the Ni crystallite followed by the nucleation and growth of carbon filaments (e.g., whiskers).

The studies concerning carbon formation over Ni and Co-based catalysts during SR of ethanol are more scarce and the mechanism is not well understood. Typically, two types of carbonaceous deposits have been reported in the literature: amorphous carbon and filamentous carbon [31–34]. The nature of carbon formed depends on the reaction conditions.

We carried out TG and TEM analyses in order to study the effect of reaction conditions on the nature of the carbon deposits formed. This may provide useful guidance in determining the optimal operating conditions that minimize coke formation during ethanol conversion reactions for hydrogen production.

Fig. 11 shows the TPO profile of the Co/CeO_2 catalyst after different reaction conditions. The TPO profile exhibited one peak in the range of 721–730 K and a shoulder positioned at 753–760 K after subjecting the catalyst to SR reaction under different H_2O/ethanol molar ratios. In addition, increasing the H_2O/ethanol molar ratio from 3.0 to 10.0 decreased the intensity of the peak at low temperature. After POX and OSR, one narrow peak and one broad peak were observed at approximately 719 and 765 K, respectively. The TPO profile did not exhibit weight loss following SR at 1073 K.

The amounts of carbon deposited on the Co/CeO_2 catalyst after exposure to different reaction conditions are listed in Table 1. The amount of carbon deposited on the catalyst after SR at 773 K and H_2O/ethanol molar ratio of 3.0 was higher than the one observed after POX and OSR at 773 K. Increasing the H_2O/ethanol molar ratio from 3.0 to 10.0 resulted in a decrease in the amount of carbon deposited on the catalyst surface following SR at 773 K. Carbon deposition was no longer observed during SR at high temperature.

These two different oxidation regions can be due to the presence of two different types of carbon on the surface of the catalyst.

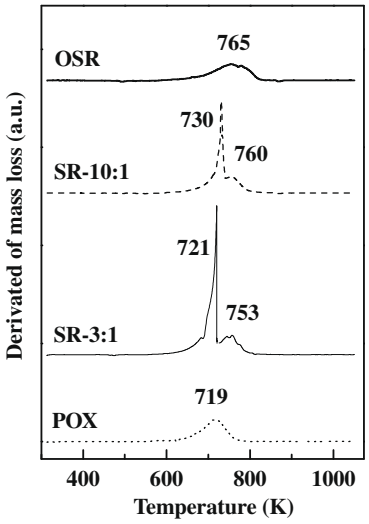

Fig. 11. TPO profile of 10% Co/CeO_2 catalyst obtained after subjecting the catalyst to different reaction conditions.

Table 1
Amount of carbon deposited on the catalyst surface as determined by TGA after exposing the catalyst to different reaction conditions. During TGA, 5%O_2:He mixture and a heating rate of 10 K/min were used.

Reaction condition	mg carbon/g catalyst/h
SR at 773 K under H_2O/ethanol molar ratio = 3.0	4.3
SR at 773 K under H_2O/ethanol molar ratio = 10.0	2.3
POX at 773 K under O_2/ethanol = 0.5	1.8
OSR at 773 K under H_2O/ethanol molar ratio = 3.0 and O_2/ethanol molar ratio = 0.5	1.5
SR at 1073 K under H_2O/ethanol molar ratio = 3.0	0.0

The group of Prof. Resasco regularly uses TPO as an important tool to characterize the types of carbonaceous species present on Co-based catalysts used in the production of carbon nanotubes [50]. The oxidation peak located below 673 K is ascribed to amorphous carbon, whereas the peak above 773 K corresponds to carbon nanotubes. The oxidation of graphite occurs at higher temperatures (~973 K).

There are few studies available in the open literature that made use of TPO after SR of ethanol to study the nature of carbonaceous deposits and to quantify the amount of carbon formed over supported Co catalysts [17,26,31,34]. Wang et al. [34] performed TG analyses after SR of ethanol at different reaction temperatures over Co/CeO_2. The TPO profile after SR at 773 K displayed two peaks at around 698 and 848 K, while no peaks were detected during TGA following SR at 873–973 K. However, the authors did not correlate these peaks to the types of carbonaceous species formed. Two peaks at 573 and 773 K were also present in the TPO profile of $Co/CeZrO_2$ catalyst after SR of ethanol at 813 K [31]. They were attributed to carbonaceous deposits over the surfaces of the particles and to carbon filaments. The TPO profile of $CoRh/SiO_2$ catalyst following OSR at 673 K exhibited two peaks below 673 K but they were not assigned to any particular carbon species [17]. No TGA or TPO results following exposure of a Co-based catalyst to the POX reaction were found in the literature.

Using the TPO peak assignments from the literature as a basis, our TPO profile indicates the presence of amorphous carbon and filamentous carbon over the Co/CeO_2 catalyst after running SR under H_2O/ethanol ratios of 3.0 and 10.0 and following exposure to OSR reaction. In addition, the fraction of amorphous carbon appears to be higher in the cases of SR as compared to OSR.

Electron microscopy techniques have been used to characterize the nature of the carbonaceous species formed over Co-based cat-

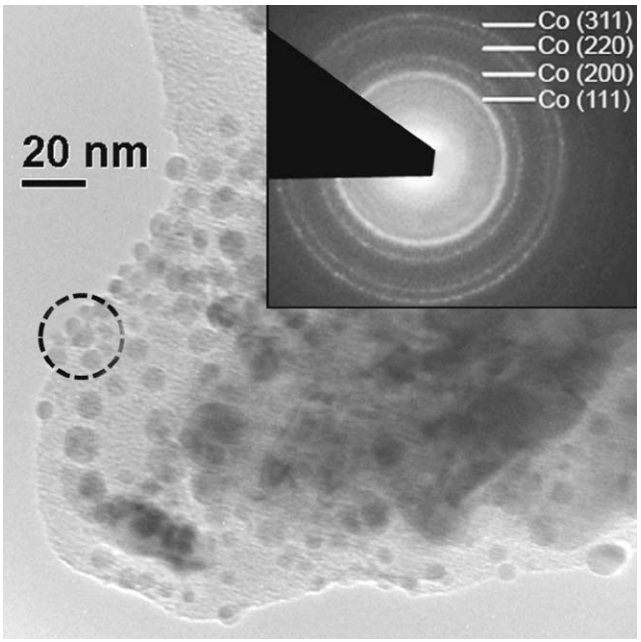

Fig. 13. HR-TEM image of the Co/CeO_2 catalyst reduced at 1023 K and passivated under an O_2/He mixture. The inset corresponds to selected area electron diffraction patterns recorded on cobalt particle.

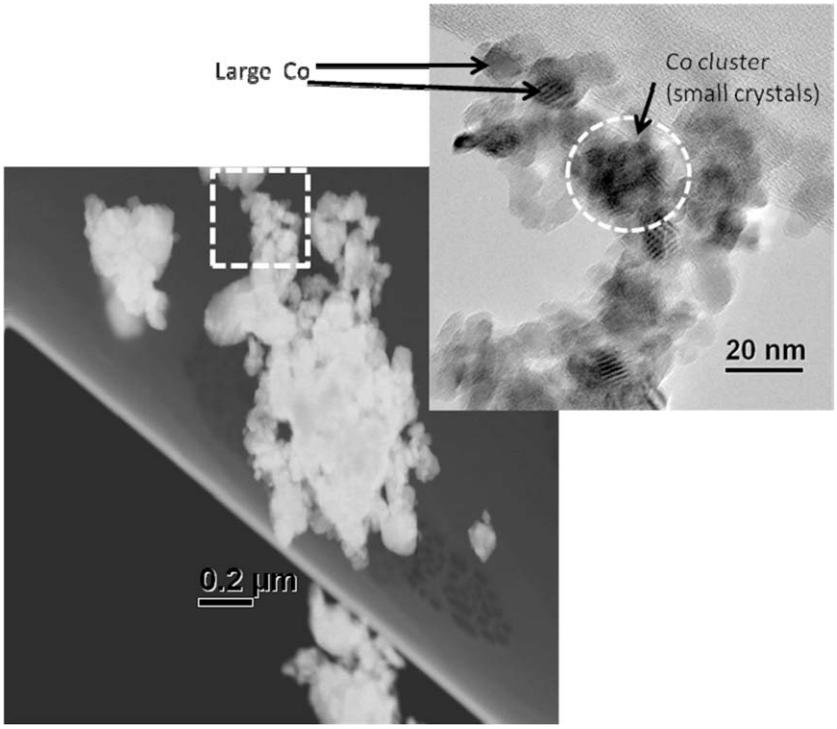

Fig. 12. STEM and HR-TEM images of the Co/CeO_2 catalyst reduced at 1023 K and passivated under an O_2/He mixture.

alysts during SR. HR-TEM images of Co/CeO_2 catalyst following SR of ethanol at 723 K displayed Co particles covered by amorphous carbon with a minor amount extending over the support [28]. TEM analyses revealed the presence of two types of carbon deposits on $Co/CeZrO_2$ catalyst after SR at 813 K: a carbonaceous layer residing on the surface of the metallic particle, and carbon filaments. Galetti et al. [33] observed that the morphologies of the spent catalysts varied significantly as a function of reaction temperature. Carbon filaments were detected by SEM on the surface of CuCoZnAl catalyst after SR of ethanol at 773 K, but were absent in images taken after reaction at 873 K. Wang et al. [34] also concluded that the nature of carbon deposits during SR over Co/CeO_2 catalyst is dependent on the reaction temperature. TEM images revealed the presence of carbon encapsulating the cobalt particle when the reaction was performed at 623 and 723 K, resulting in severe deactivation. On the other hand, at 773 and 823 K, carbon filaments were detected but the catalyst did not deactivate. At high reaction temperature (973 K), carbon deposits were not observed and the catalyst remained stable.

In our work, TEM images were carried out after different reaction conditions to shed light on the mechanism of carbon formation over Co/CeO_2. Figs. 12–16 display TEM micrographs of the Co/CeO_2 catalyst after exposure to different reaction conditions.

Fig. 12 displays the STEM image of the Co/CeO_2 catalyst reduced in hydrogen and passivated under an O_2/He mixture. After reduction, cobalt particles are formed in a size range from 3 nm up to 20 nm with the majority of particles ranging between 5 and 10 nm in size. The largest Co particles can be identified in HR-TEM to actually be a composite of several smaller Co crystals. The Co catalyst particles have a hexagonal or pseudo-hexagonal morphology as shown by the HR-TEM inset in Fig. 12. A represen-

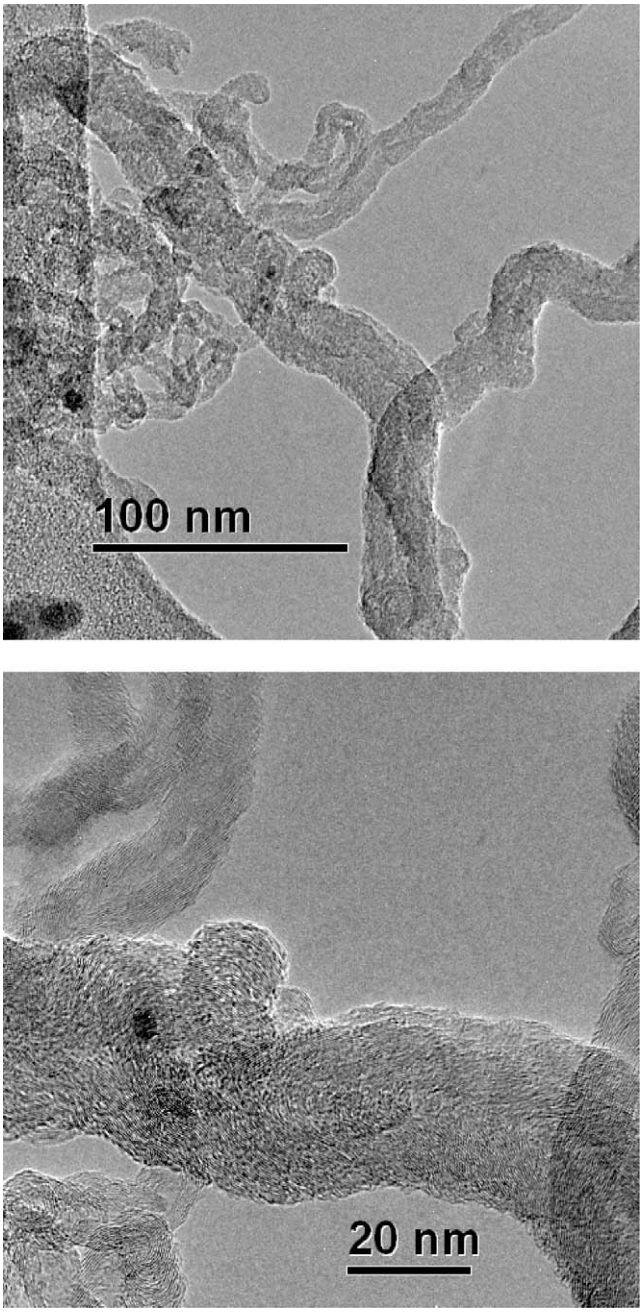

Fig. 14. HR-TEM images of the Co/CeO_2 following SR under H_2O/ethanol molar ratio = 3.0 at 773 K.

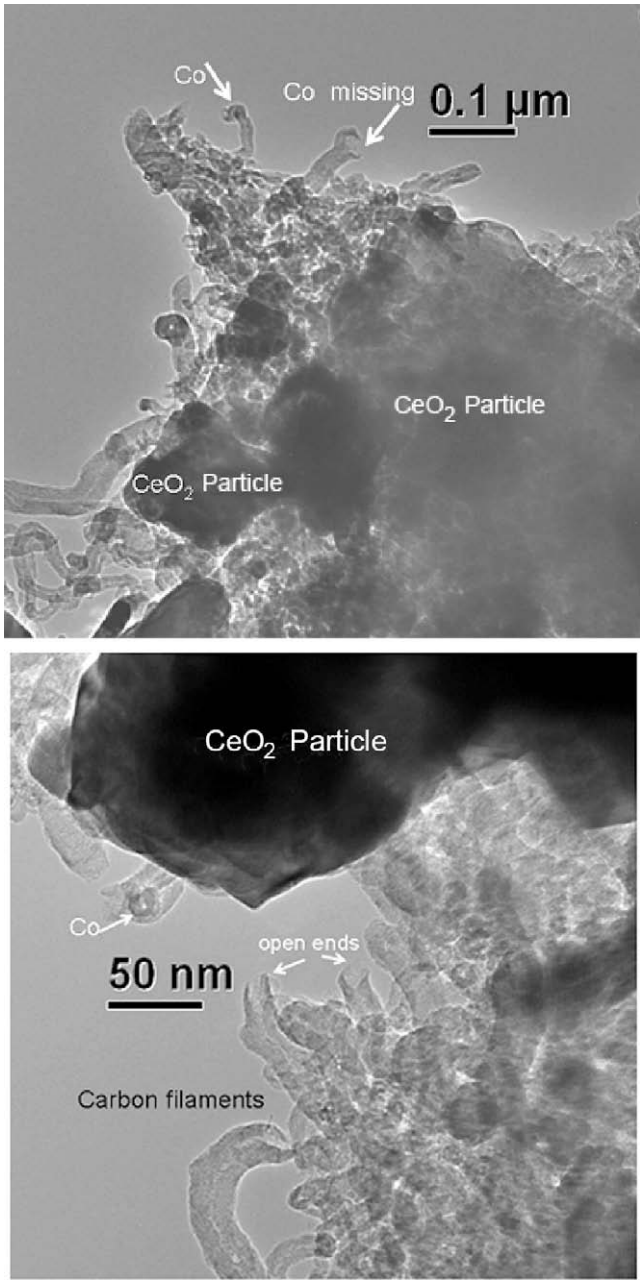

Fig. 15. HR-TEM images of the Co/CeO_2 following OSR under H_2O/ethanol molar ratio = 3.0 and O_2/ethanol molar ratio = 0.5 at 773 K.

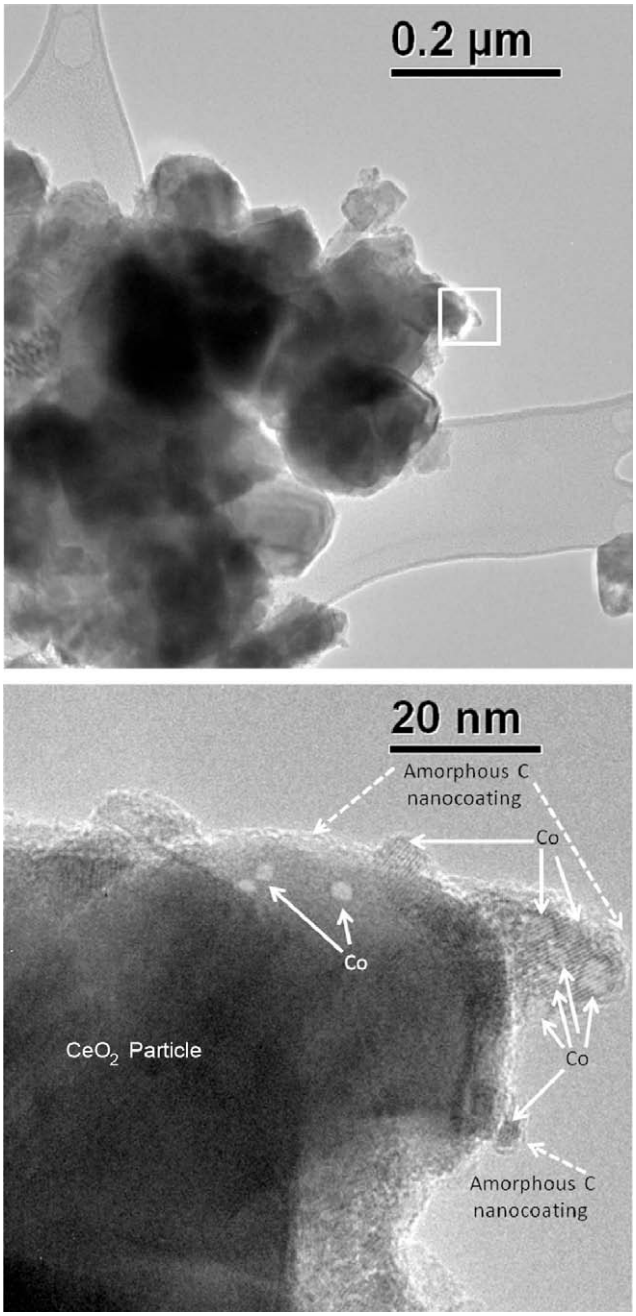

Fig. 16. HR-TEM images of the Co/CeO_2 following SR under H_2O/ethanol molar ratio = 3.0 at 1073 K.

tative diffraction pattern for the cobalt nanoparticles was obtained during the TEM investigation, displaying characteristic rings for a Co^0 phase (Fig. 13). The arrangement of concentric rings (diffraction pattern was obtained from several randomly oriented cobalt particles) corresponds to the presence of the Co (111), (200), (220), and (310) planes assigned to Co^0 confirming our conclusion that reduction indeed leads to the formation of cobalt metal nanoparticles. In addition, the EELS spectra of the Co nanoparticle showed the L_2/L_3 edges with a typical intensity difference for L_2 and L_3 characteristic of Co^0 (L_3 is significantly taller compared with L_2). Furthermore, the oxygen K-edge is missing in the spectra at 530 eV.

Ceria nanoparticles are typically agglomerated in spent catalysts. The individual ceria grain sizes are on the order of 4–10 nm while ceria agglomerates can be observed in excess of 0.5 μm.

The images of Co/CeO_2 catalyst following exposure to SR under H_2O/ethanol ratios of 3.0 and OSR at 773 K are shown in Figs. 14 and 15 and illustrate the presence of carbon deposits, which are always in proximity to the Co particles.

Cobalt catalyst nanoparticles in the spent catalyst are well-crystallized (hexagonal and pseudo-hexagonal crystals), ranging from ~3 to 30 nm in size and are located on the ceria agglomerates. The larger Co particles appear to have formed from close spatial arrangements of several <5 nm particles. Most importantly, Co nanoparticles occur in either of two spatial arrangements: (1) dispersed on ceria surfaces and in this case, lesser amounts of carbon deposits formed nanocoatings on the Co and CeO_2 exterior; or (2) alternately, a high fraction of Co nanoparticles occur separated from the CeO_2 host surface (Co must have been lifted off the support) and in this case, those Co nanoparticles initiated the formation of carbon tubular nanostructures shown in Fig. 14 (Co particles are located at the ends of carbon tubules). The carbon tubular morphology entails multiple outer walls which are not parallel to the inner channel, but rather in a configuration best described as a herringbone structure with numerous capped areas that disrupt or cap the inner channel. Thus the carbon nanostructures are not carbon nanotubes, but resemble more likely carbon nanofibers or filaments.

The relative sizes (i.e., diameters) of the carbon nanostructures are clearly controlled by the Co nanoparticle size. In some instances, two or more Co nanoparticles form a larger cluster that initiates the growth of rather large carbon nanotubular structures with diameters of up to 35 nm. Several carbon nanotubular structures also engulfed ultra small (typically <3 nm) Co nano-catalyst particles as shown in Fig. 14b. Therefore, some of the Co is confined to the internal structure of the carbon nanotubular host. In addition, several carbon filaments are characterized by an open end where a Co nanoparticle became detached as illustrated in Fig. 15a and b. The morphology of the carbon tubular nanostructures or filaments was observed to be similar in both samples, but the frequency and location of the carbon deposits vary significantly. Carbon nanostructures were not detected over the Co/CeO_2 catalyst following SR at 1073 K (Fig. 16). In this case, some regions revealed only the presence of amorphous carbon in proximity to the ceria agglomerates. Fig. 16a shows a large ceria agglomerate and under high magnification (Fig. 16b) one can observe well-crystallized cobalt catalyst particles on the ceria surface. The cobalt catalyst particles clustered to form an approximately 20 nm grain which is overgrown by a very thin (~2–3 nm) layer of amorphous carbon nanocoating.

According to the proposed reaction mechanism based on DRIFTS experiments over Co/CeO_2 catalyst under different reaction conditions, the decomposition of dehydrogenated species (e.g., acetaldehyde, acetyl) and acetate species produce hydrogen, CO, and CH_x species, which may in turn result in carbon formation depending on the rate of hydrogen recombination. We have recently demonstrated that the presence of the metal promotes the decomposition of acetate species over $Pt/CeZrO_2$ catalyst [16]. Therefore, the catalyst should deactivate when the rate of this reaction pathway is higher than the rate of desorption of CH_x species as CH_4. The CH_x species formed may block the Pt-support interface resulting in catalyst deactivation. The CH_x species may be further dehydrogenated to H and C. In the case of Co-based catalysts, the formed carbon will either (a) diffuse behind the metal to assist in carbon filament growth or (b) react with O_2 (or H_2O) to produce CO_X species (Scheme 1). The addition of an excess of water or oxygen to the feed helps to clean the surface of the metal, keeping it active for a longer period of time. Therefore, the metal can remain active despite having a considerable amount of carbon deposited behind the particles, since the top surface will remain exposed to reactants and gas-phase intermediates. According to

Trimm [47], this is a special case where the coke formation does not result in catalyst deactivation.

When SR is carried out at high temperature (1073 K), carbon does not accumulate, and this may be due to: (1) the steam and CO_2 reforming of methane reactions; (2) the reverse of the disproportion reaction (Eq. 7); and/or (3) the carbon gasification reaction, which is favored at high temperatures.

4. Conclusions

DRIFTS, reaction testing, and TPD measurements provided the following conclusions regarding the reaction network. With ED, ethanol adsorbs dissociatively at low temperature to form adsorbed ethoxy species and a bridging –OH group. At moderate temperatures, ethoxy species diminish and acetaldehyde increases. A fraction of the ethanol decomposes to H_2, CH_4, and CO, and another fraction dehydrogenates to acetaldehyde. At higher temperatures, acetaldehyde is converted to acetate via support bound –OH groups. In the absence of steam, the dehydration product of ethylene is favored.

With SR, OSR, and POX, the increased coverage of –OH and lattice O adatoms promotes the formation of acetate at lower temperatures. At higher temperatures, steam promotes the forward decomposition of acetate to carbonate and CH_4, the latter of which decomposes over Co metal particles to evolve H_2 and carbon. Replacing steam with oxygen resulted in losses in H_2 selectivity as the forward decomposition was hindered; thus, higher acetaldehyde production was observed. In OSR, although acetaldehyde production was inhibited by the presence of H_2O in the feed, the H_2 selectivity was lower relative to the case of SR alone.

Regarding catalyst stability, the reaction type, feed ratios, and temperature strongly influence the nature of the carbon deposits that form and their impact on catalyst stability. The results suggest that the carbon diffuses behind the particle, nucleating the growth of carbon filaments. The filamentous carbon lifts the Co particles from the support, but this does not directly lead to catalyst deactivation. In cases where high H_2O/ethanol feed ratios are employed, or if oxygen is included in the feed, enough of the active surfaces of both the support and metal remains exposed and accessible to reactants and intermediates, such that the catalyst deactivation rate is alleviated. On the other hand, when less of H_2O or no oxygen was present, amorphous carbon tended to cover and block active sites, leading to more significant losses in activity.

Acknowledgments

This work received financial support of CTENERG/FINEP-01.04.0525.00. CAER acknowledges the Commonwealth of Kentucky for financial support.

References

[1] P.R. de la Piscina, N. Homs, Chem. Soc. Rev. 37 (2008) 2459.
[2] P.D. Vaidya, A.E. Rodrigues, Ind. Eng. Chem. Res. 45 (2006) 6614.
[3] A. Haryanto, S. Fernando, N. Murali, S. Adhikari, Energy Fuels 19 (2005) 2098.
[4] H. Song, L. Zhang, R.B. Watson, D. Braden, U.S. Ozkan, Catal. Today 129 (2007) 346.
[5] R.M. Navarro, M.C. Alvarez-Galvan, M.C. Sanchez-Sanchez, F. Rosa, J.L.G. Fierro, Appl. Catal. B 55 (2004) 223.
[6] M. Veronica, B. Graciela, A. Norma, L. Miguel, Chem. Eng. J. 138 (2008) 602.
[7] A.N. Fatsikostas, X.E. Verykios, J. Catal. 225 (2004) 439.
[8] A. Erdohelyi, J. Raskó, T. Kecskés, M. Tóth, M. Dömök, K. Baán, Catal. Today 116 (2006) 367.
[9] V. Fierro, V. Klouz, O. Akdim, C. Mirodatos, Catal. Today 75 (2002) 141.
[10] L.V. Mattos, F.B. Noronha, J. Power Sources 145 (2005) 10.
[11] L.V. Mattos, F.B. Noronha, J. Power Sources 152 (2005) 50.
[12] L.V. Mattos, F.B. Noronha, J. Catal. 233 (2005) 453.
[13] J.L. Bi, S.N. Hsu, C.T. Yeh, C.B. Wang, Catal. Today 129 (2007) 330.
[14] J. Kugai, S. Velu, C. Song, Catal. Lett. 101 (2005) 255.
[15] V. Fierro, O. Akidim, C. Mirodatos, Green Chem. 5 (2003) 20.
[16] S.M. de Lima, I.O. da Cruz, G. Jacobs, B.H. Davis, L.V. Mattos, F.B. Noronha, J. Catal. 257 (2008) 356.
[17] E.B. Pereira, N. Homs, S. Marti, J.L.G. Fierro, P.R. de la Piscina, J. Catal. 257 (2008) 206.
[18] N. Laosiripojana, S. Assabumrungrat, Appl. Catal. B 66 (2006) 29.
[19] T. Nishiguchi, T. Matsumoto, H. Kanai, K. Utani, Y. Matsumurab, W-J. Shenc, S. Imamura, Appl. Catal. A 279 (2005) 273.
[20] J. Llorca, N. Homs, P.R. de la Piscina, J. Catal. 227 (2004) 556.
[21] J. Llorca, P.R. de la Piscina, J. Sales, N. Homs, Chem. Commun. (2001) 641.
[22] W. Cai, F. Wanga, E. Zhan, A.C. Van Veen, C. Mirodatos, W. Shen, J. Catal. 257 (2008) 96.
[23] J. Kugai, V. Subramani, C. Song, M.H. Engelhard, Y.H. Chin, J. Catal. 238 (2006) 430.
[24] H. Roh, A. Platon, Y. Wang, D.L. King, Catal. Lett. 110 (2006) 1.
[25] G. Jacobs, R.A. Keogh, B.H. Davis, J. Catal. 245 (2007) 326.
[26] F. Romero-Sarria, J.C. Vargas, A. Roger, A. Kiennemann, Catal. Today 133 (2008) 149.
[27] L.P.R. Profeti, E.A. Ticianelli, E.M. Assaf, J. Power Sources 175 (2008) 482.
[28] J. Llorca, N. Homs, J. Sales, P.R. de la Piscina, J. Catal. 209 (2002) 306.
[29] B. Zhang, X. Tang, Y. Li, W. Cai, Y. Xu, W. Shen, Catal. Commun. 7 (2006) 367.
[30] H. Wang, J.L. Ye, Y. Liu, Y.D. Lin, Y.N. Qin, Catal. Today 129 (2007) 305.
[31] J.C. Vargas, S. Libs, A.C. Roger, A. Kiennemann, Catal. Today 107 (2005) 417.
[32] J.M. Guil, N. Homs, J. Llorca, P.R. de la Piscina, J. Phys. Chem. B 109 (2005) 10813.
[33] A.E. Galetti, M.F. Gomez, L.A. Arrua, A.J. Marchi, M.C. Abello, Catal. Commun. 9 (2008) 1201.
[34] H. Wang, Y. Liu, L. Wang, Y.N. Qin, Chem. Eng. J. 145 (2008) 25.
[35] S. Cavallaro, V. Chiodo, A. Vita, S. Freni, J. Power Sources 123 (2003) 10.
[36] P. Gajardo, P. Grange, B. Dalmon, J. Phys. Chem. 83 (1979) 1771.
[37] F.B. Noronha, C.A. Perez, R. Frety, M. Schmal, Phys. Chem. Chem. Phys. 1 (1999) 2861.
[38] G. Jacobs, E. Chenu, P.M. Patterson, L. Calico-Williams, D.E. Sparks, G. Thomas, B.H. Davis, Appl. Catal. A 258 (2004) 203.
[39] E.M. Cordi, J.L. Falconer, J. Catal. 162 (1996) 104.
[40] L.F. de Mello, F.B. Noronha, M. Schmal, J. Catal. 220 (2003) 358.
[41] A. Yee, S.J. Morrison, H. Idriss, J. Catal. 191 (2000) 30.
[42] J. Raskó, A. Hancz, A. Erdohelyi, Appl. Catal. A 269 (2004) 13.
[43] M. Mavrikakis, M.A. Barteau, J. Mol. Catal. A: Chem. 131 (1998) 135.
[44] P.V. Menacherry, G.L. Haller, J. Catal. 177 (1998) 175.
[45] H. Song, U.S. Ozkan, J. Catal. 261 (2009) 66.
[46] M. Dömök, M. Tóth, J. Raskó, A. Erdohelyi, Appl. Catal. B 69 (2007) 262.
[47] D.L. Trimm, Catal. Today 37 (1997) 233.
[48] D.L. Trimm, Catal. Today 49 (1999) 49.
[49] R.M. Navarro, M.A. Pena, J.L.G. Fierro, Chem. Rev. 107 (2007) 3952.
[50] B. Kitiyanan, W.E. Alvarez, J.H. Harwell, D.E. Resasco, Chem. Phys. Lett. 317 (2000) 497.